Acta Cryst. (1973). A**29**, 529

High-Resolution Dark-Field Electron Microscopy. I. Useful Approximations

BY J. M. COWLEY
Department of Physics, Arizona State University, Tempe, Arizona 85281, *U.S.A.*

(*Received* 12 *December* 1972; *accepted* 9 *April* 1973)

Simple expressions are derived for the form of the intensity distributions in high-resolution dark-field electron micrographs of thin specimens for which the phase-object approximation may be applied. For cases in which the phase change of the electron wave can be assumed to be small it is shown that there is an optimum defocus value which gives the best, interpretable resolution. For dark-field images obtained either with a central beam stop or with a tilted incident beam, the image intensity is shown to depend on the square of the deviation of the projected potential from an average value. The further complications resulting when the phase change cannot be assumed small are discussed and illustrated by means of a simple example.

1. Introduction

In recent years some important results have been obtained by the use of dark-field microscopy under conditions of high resolution. Although in comparison with bright-field imaging the method suffers because the increased exposure times required result in more serious radiation damage effects on the specimen, it is valuable in many cases because of the increased contrast possible from very thin specimens.

By use of the 'high-resolution dark-field' technique with a tilted incident beam, Hashimoto, Kumao, Hino, Yotsumoto & Ono (1971) obtained images showing, apparently, individual heavy atoms, similar to the images obtained by Crewe & Wall (1970), who used scanning transmission electron microscopy (STEM) with a combination of an elastic-scattering dark-field image signal and an inelastic-scattering dark-field signal. Formanek, Muller, Hahn & Koller (1971) showed similar images in bright field. Highly successful applications of dark-field techniques for thin biological specimens have been made by Massover (1972) using the 3MeV electron microscope at Toulouse (Dupuoy, Perrier & Durrieu, 1970). Various dark-field techniques, some involving annular apertures, have been developed by Heinemann & Poppa (1970) for revealing the lattice periodicities of thin metal crystals. Dark-field images from the diffuse scattering given in disordered materials have been used by various authors in attempts to derive information about the microstructure of amorphous solids and disordered alloys.

For bright-field electron microscopy of thin objects with high resolution (minimum resolvable distance less than about 20 Å) it is now well established that the microscope image contrast can be predicted or interpreted on the basis of the approximation which treats the specimen as a thin phase object, with some small absorption effect included for improved accuracy. Amplitude contrast in the image is then obtained by an "optimum defocusing' of the objective lens. The limitations of specimen thickness and phase change for which this approximation is valid have been explored by detailed calculations of image intensities of model systems by Grinton & Cowley (1971). The application of this concept to the interpretation of high-resolution images of crystal lattices of inorganic oxides (Iijima, 1971), where the phase change of the electron wave cannot be assumed to be small, has been explored by Cowley & Iijima (1972).

For dark-field images an equivalent understanding of the contrast effects does not exist. For the most part authors seem to have relied on the simple, intuitively appealing concept that the dark-field image intensity is proportional to the scattering density in the object and is almost independent of focus. The aim of this paper is to demonstrate that in many cases this simple interpretation is wrong and may lead to serious errors in the deductions made regarding object structure.

2. Thin-phase-object image theory

The transmission function for a phase object is written

$$q(xy)=\exp\{-i\sigma\varphi(xy)\}\,, \qquad (1)$$

where $\sigma=\pi/\lambda E$, E is the accelerating voltage and relativistically corrected values of λ and E are assumed. The projection of the potential distribution of the object in the beam direction is

$$\varphi(xy)=\int\varphi(\mathbf{r})\mathrm{d}z\,. \qquad (2)$$

The effect of the object on a coherent incident electron wave is represented by multiplying the incident wave function by (1). This approximation ignores the spread of the wave inside the object by Fresnel diffraction and is valid for specimen thicknesses which depend on the wavelength, the resolution and the accuracy of the desired result but are of the order of 100 Å for 3 Å resolution (Cowley & Iijima, 1972) or 300–500 Å for 6 Å resolution (Grinton & Cowley 1971).

For an incident wave of amplitude unity the distribution of amplitude on the back focal plane of an ideal lens is given by the Fourier transform ($\mathscr{F}$) of (1) as

$$\psi(uv)=Q(uv)=\mathscr{F}[\exp\{-i\sigma\varphi(xy)\}]\,, \qquad (3)$$

where capital letters are used for reciprocal-space functions of the coordinates u,v. For an ideal thin lens of focal length $f, u=x/f\lambda$ and $v=y/f\lambda$.

The effects of finite aperture and imperfections of the lens are included by multiplying (3) by an aperture function $A(uv)$ and a phase function

$$\exp[-i\chi(uv)]\,.$$

It can be shown that for near-focus image the effect of the aperture function may be approximated by adding an effective absorption term, *i.e.* by making $\varphi(xy)$ complex (Grinton & Cowley, 1971) or by multiplying (1) by $\exp\{-\mu(xy)\}$. For the small aperture sizes used in normal low-resolution biological electron microscopy this term becomes the main source of contrast but it decreases as the aperture size increases and may be ignored as a first approximation for high-resolution imaging.

In the phase term modulating (3), we may write

$$\chi(uv)=\pi R\lambda U^2-\frac{\pi}{2}C_s\lambda^3U^4, \qquad (4)$$

where, on the right-hand side, U is used as a radial coordinate $[=(u^2+v^2)^{1/2}]$. The second-order term in U represents the effect of defocus (under focus) by a distance R referred to the specimen. The fourth-order term arises from spherical aberration of the lens. We ignore the effects of other aberrations such as astgimatism which may be made negligible.

If we now make the 'weak phase object' approximation, as used in consideration of very thin biological specimens or the imaging of single atoms (Scherzer, 1949; Heidenreich & Hamming, 1965; Eisenhandler & Siegel, 1965; Erickson & Klug, 1970), we assume $\sigma\varphi(xy)\ll 1$; then (1) becomes

$$q(xy)=1-i\sigma\varphi(xy)\,,$$

and, including the phase term, (3) becomes

$$\psi(uv)=\delta(uv)-\sigma\Phi(uv)\sin\chi-i\sigma\Phi(uv)\cos\chi\,, \qquad (5)$$

or, with absorption,

$$\psi(uv)=[\delta(uv)-\sigma\Phi(uv)\sin\chi-M(uv)\cos\chi] - i[\sigma\Phi(uv)\cos\chi-M(uv)\sin\chi]\,. \qquad (6)$$

where $M(uv)=\mathscr{F}\mu(xy)$.

Considering (5) only, it is seen that ideal imaging conditions would result for $\chi=\pi/2$ for all U so that $\sin\chi=1$ and the image amplitude would be given by Fourier transform of (5) as

$$\psi_i(xy)+1-\sigma\varphi\left(-\frac{x}{M},-\frac{y}{M}\right),$$

where $-M$ is the magnification factor. The image intensity would then be, to first order in $\sigma\varphi$,

$$I(xy)=|\psi(xy)|^2=1-2\sigma\varphi\left(-\frac{x}{M},-\frac{y}{M}\right)\,. \qquad (7)$$

As is well known, a reasonable approximation to this ideal situation is achieved for an optimum defocus, R. In Fig. 1 the values of $\sin\chi$ and $\cos\chi$ are plotted for the value of $C_s=1\cdot8$ mm, which is appropriate for a good modern electron microscope. For R values of 900 to 1000 Å the value of $\sin\chi$ is close to unity for a large part of the range of U which is of interest. The fact that in this range the value of $\cos\chi$ varies strongly

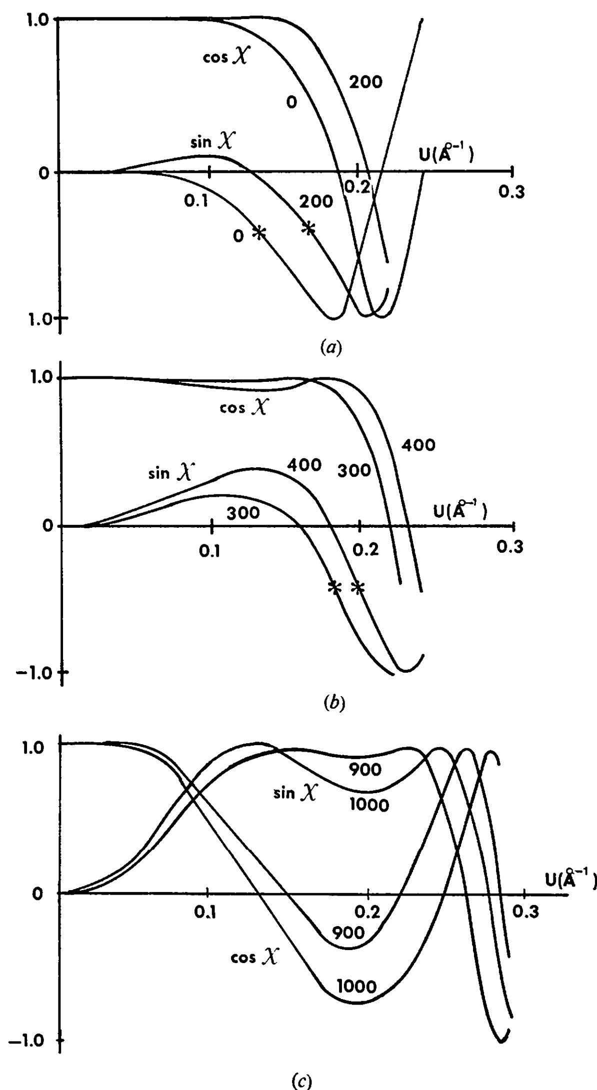

Fig. 1. Variation of $\sin\chi$ and $\cos\chi$ with U, the radial coordinate in reciprocal space, where χ is the phase factor due to defocus, R, and spherical aberration with $C_s=1\cdot8$ mm. Curves are drawn for (*a*) $R=0$ and -200 Å, (*b*) $R=-300$ and -400 Å, (*c*) $R=-900$ and -1000 Å.

is not important because the imaginary part of (5) can contribute only second-order terms to the image intensity. However, the fact that $\cos\chi \simeq 1$ for small U values means that the effect of the absorption included as in (6) will compensate partly for the low values of $\sin\chi$ in this region since $-M(uv)$ will have roughly the same form as $\sigma\Phi(uv)$.

The favorable form of the image contrast for bright-field images given by (7) is obviously the result of combining the Fourier transform of the projected potential and the δ function representing the transmitted beam, with the correct phase relationship. In dark-field imaging the same consideration cannot apply since the transmitted-beam δ function is excluded. The oversimplified view of dark-field images is then that by making $\chi \simeq 0$, (5) becomes $\psi(uv) = -i\sigma\Phi(uv)$ and the image intensity is

$$I(xy) = \sigma^2\varphi^2(xy)\,. \tag{8}$$

However, in addition to the central δ function due to the incident beam, other important parts of the diffraction pattern are inevitably excluded, including $i\sigma\Phi(0,0)$,

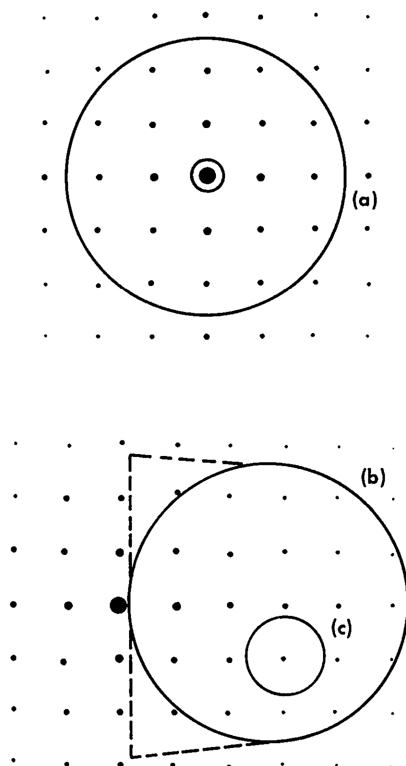

Fig. 2. (*a*) The 'ideal' dark-field condition in which a small central stop intercepts the central beam of the diffraction pattern but all the rest of the diffraction pattern within a large aperture is transmitted. (*b*) The translated aperture or 'high-resolution dark-field' condition in which the aperture excludes the central beam. Dotted lines suggest the approximation used to derive a rough model for the effects of such an aperture. (*c*) A small aperture well displaced from the central beam.

the forward-scattered beam which is always the strongest part of the diffraction pattern. Hence in order to make more realistic estimates of dark-field contrast we must consider the effects of selecting only particular parts of the diffraction pattern to contribute to the image.

3. 'Ideal' dark field–central stop

The form of dark-field image which might be considered to give the most easily interpreted contrast is the idealized case in which a very small central stop intercepts the central bright spot of the diffraction pattern but very little else, as in Fig. 2(*a*). In the approximation of (5), the transmitted beam, $\delta(uv)$ and the forward scattering maximum, of strength $-i\sigma\Phi(0,0)$ are excluded.

Apart from this omission the diffraction pattern amplitude is

$$-i\sigma\varphi(uv)\,.\,\exp\{i\chi(uv)\}\,.$$

The requirement for a readily interpreted image is that $\cos\chi(uv)$ and $\sin\chi(uv)$ should be almost constant over the range of U of interest. This condition is obviously not satisfied for the bright-field optimum defocus condition, Fig. 1(*c*). For zero defocus $\cos\chi$ is nearly unity out to $U=0{\cdot}16$ Å^{-1} but $\sin\chi$ deviates by 0·3 (which we take as an arbitrary limitation) for $U=0{\cdot}13$ Å^{-1}. An improved situation exists with increasing R, with an optimum value of R of about 400 Å for which $\cos\chi \simeq 1$ and $|\sin\chi| < 0{\cdot}3$ for $U \le 0{\cdot}2$ Å^{-1}. Then for resolutions of about 5 Å in the image we may assume as a first approximation for this optimum dark field defocus that $\chi \simeq 0$.

The effect of the central stop is illustrated best for a periodic object,

$$\varphi(xy) = \sum_h\sum_k\Phi_{hk}\exp\left\{2\pi i\left(\frac{hx}{a} + \frac{ky}{b}\right)\right\}. \tag{9}$$

The diffraction pattern is a set of δ functions:

$$\Phi(uv) = \sum_h\sum_k\Phi_{hk}\delta\left(u - \frac{h}{a}, v - \frac{k}{b}\right). \tag{10}$$

The central stop then eliminates the unscattered beam, $\delta(uv)$, plus the zero-order beam $-i\sigma\Phi_{00}\delta(uv)$. The image amplitude and intensity are then (apart from the magnification term):

$$\psi(xy) = -i\sigma[\varphi(xy) - \Phi_{00}]\,. \tag{11}$$

$$I(xy) = \sigma^2|\varphi(xy) - \Phi_{00}|^2. \tag{12}$$

But $\Phi_{00} = \int \varphi(xy)\mathrm{d}x\mathrm{d}y$, where the integration is over the unit cell. Similarly for non-periodic objects $\Phi_{00} = \bar{\varphi}$, the average of the potential projection over a coherently illuminated region. Thus the image intensity is not a simple representation of the scattering density. In particular it is seen that both positive and negative deviations from an average projected potential will give intensity maxima.

As a simple, familiar example, we consider the case of a projected potential of the form

$$\varphi(xy)=A+B\cos(2\pi x/a)\,.$$

The distribution in the back focal plane will be

$$\psi(u,v)=\delta(uv)[1-i\sigma A]-\frac{i\sigma}{2}B\left[\delta\left(u-\frac{1}{a}\right)+\delta\left(u+\frac{1}{a}\right)\right].$$

The ideal dark-field amplitude and intensity are

$$\psi(xy)=-i\sigma B\cos(2\pi x/a)\,,$$

$$I(xy)=\sigma^2B^2\cos^2(2\pi x/a)\,.$$

Thus the image intensity has half the periodicity of $\varphi(xy)$.

For more complicated structures the periodicity may possibly be reduced but cannot be increased. False impressions will be given of details of objects except in the case of sharp isolated potential maxima, *e.g.* well separated heavy atoms on a thin light-atom support.

It is to be expected that the value of $\varphi(xy)-\bar{\varphi}$ will usually pass through zero around the base of any isolated prominent maximum or minimum of $\varphi(xy)$. Hence bright peaks in the intensity distribution will tend to be surrounded by dark rings.

Some modification of the above considerations must be made in practice to take account of the finite size of the central beam stop which is used. A disc of finite size will remove some of the diffraction pattern surrounding the zero-order reflection. This is equivalent to multiplying $\psi(uv)$ by

$$S(uv)=\begin{cases}1 \text{ if } U>A/2\\ 0 \text{ if } U<A/2\,.\end{cases}$$

Thus the image amplitude is convoluted with

$$s(xy)=\delta(xy)-J_1(\pi Ar)/(\pi r)\,,$$

where

$$r=(x^2+y^2)^{1/2}\,.$$

Instead of Φ_{00} in (11) we then have

$$\varphi(xy)*J_1(\pi Ar)/(\pi r)$$

which tends to Φ_{00} as $A\to 0$.

The implication of this convolution is that the average $\bar{\varphi}$ is taken over an area of diameter approximately equal to A^{-1}. For example, the center of a dark field of a hole in a thin film will appear bright if its diameter D is much less than A^{-1} but it will appear dark (zero intensity) if $D\gg A^{-1}$.

An additional consideration is that the averaging of $\bar{\varphi}$ cannot be made over a region greater than the area of lateral coherence of the incident beam which is inversely proportional to the angle of convergence of the beam. This will impose no further limitation if the central-beam stop is considerably greater than the incident-beam spot in the diffraction pattern.

The presence of inelastic scattering around the incident beam position should not normally have an appreciable effect on the image intensity distribution. The small-angle inelastic scattering due to electron excitations will mostly be stopped by the central-beam stop. Wider-angle scattering which passes the beam stop will presumably have relatively large energy losses and the chromatic aberrations of the imaging lenses will ensure that this will contribute only a diffuse background to a high-resolution image.

4. Translated-aperture or 'high-resolution' dark field: large aperture

If the dark-field image is obtained by translating the objective aperture in an electron microscope or by tilting the incident-beam direction, the situation in the back focal plane can be represented as in Fig. 2(*b*), where we have taken the aperture diameter to be of roughly the same size as the maximum range of U and positioned so that it just excludes the central beam.

The most important difference between these two forms of dark-field image in practice arises from the large chromatic-aberration effects for the off-axis imaging with the translated aperture. However for high-resolution work there is an additional difference. For displaced-aperture imaging the whole aperture lies to one side of the $U=0$ point on the curves of Fig. 1, *i.e.* the diameter of the aperture must be less than the $U_{\max}$ values marked in Fig. 1 if a simple interpretation of the image is to be possible. For the tilted-beam illumination the center of the aperture is on the lens axis, the aperture function is centered at $U=0$ for these curves and the diameter of the aperture may be $2U_{\max}$. Hence for the tilted-beam 'high-resolution case' the aperture diameter over which $\chi\simeq 0$ can be twice as great, with a corresponding possible advantage in resolution.

If, as a first approximation, we assume $\chi=0$ for the aperture used, then the effect of placing an aperture asymmetrically in the diffraction pattern in the back focal plane can be represented formally by writing

$$\psi(uv)=-i\sigma\Phi(uv)\,.\,[A(U)*\delta(u-u_0)]\,,\qquad(13)$$

where $A(U)$ is a symmetrical aperture of radius less than u_0. The image intensity can then be calculated numerically by Fourier transform of (13) for any particular case. However, we prefer to seek an indication of the nature of the effects on the image, however rough, by making approximations which will provide results which can be expressed analytically.

One way of doing this to assume that the aperture used is the same as for the ideal dark-field imaging of the previous section but with half cut off by a straight edge, as suggested by the dotted outline in Fig. 2(*b*). The back-focal-plane amplitude is then

$$-i\sigma[\Phi(uv)-\Phi_{00}\delta(uv)]\,.\,H(u)\,,\qquad(14)$$

where

$$H(u)=\begin{cases}0 \text{ if } u<0\,,\\ 1 \text{ if } u\geq 0\,.\end{cases}$$

The Fourier transform of $H(u)$ is

$$h(x)=\tfrac{1}{2}\delta(x)+\frac{i}{2\pi x}\,. \tag{15}$$

The image amplitude is then convoluted by (15). But this does not lend itself to easy evaluation except numerically.

Instead we may approximate to $H(u)$ using functions which may be readily Fourier transformed, for example by the series.

$$\tfrac{1}{2}+\textstyle\sum_{n\ \mathrm{odd}} C_n U^n \exp\{-U^2/A_n^2\}\,,$$

with appropriate choice of the constants C_n and A_n. The first term of this series, $n=1$ is seen in Fig. 3 to give a reasonable approximation to $H(u)$ over the range of u values which are of most significance.

We note that we must now Fourier transform

$$\psi(uv)\,.\,u\,.\,\exp\{-u^2/A^2\}$$

and the Fourier transform of $u\ \psi(uv)$ is proportional to $\partial/\partial x\{\varphi(xy)\}$. Choosing appropriate values for C and A so that the first term of (1.6) fits $H(u)$ reasonably well from $u=0{\cdot}05$ to $0{\cdot}30$ Å^{-1}, the dark-field image amplitude may be expressed approximately as

$$\psi(xy)=\frac{\sigma}{2}\{\varphi(xy)-\bar{\varphi}\}+i\left[0{\cdot}465\left[\frac{\partial}{\partial x}\sigma\varphi(xy)\right]*\exp\{-x^2/2{\cdot}5\}\right] \tag{17}$$

and

$$I(xy)=\left[\frac{\sigma}{2}\{\varphi(xy)-\bar{\varphi}\}\right]^2+\left[0{\cdot}465\left(\frac{\partial}{\partial x}\{\sigma\varphi(xy)\}\right)*\exp\{-x^2/2{\cdot}5\}\right]^2, \tag{18}$$

where x is in Å. The convolution of the derivative with the Gaussian should give only a slight broadening of the function because the half-width of the Gaussian is only about 1·6 Å.

Hence the effect of eliminating approximately half the diffraction pattern by use of the off-center aperture can be seen to be the addition of a contribution to the image intensity proportional to the magnitude squared of the differential of $\varphi(xy)$ taken in the direction of the aperture displacement. Thus a symmetrical peak in $\varphi(xy)$ will give an intensity maximum elongated in the **x** direction. The effect could be quite similar to that of astigmatism and could possibly be 'corrected' to give a symmetrical peak by adjustment of the objective lens stigmators. As in the case of the central beam stop, the region over which $\bar{\varphi}$ is averaged in (18) will depend in practice on the lateral coherence of the incident beam and the distance from the central spot to the aperture edge.

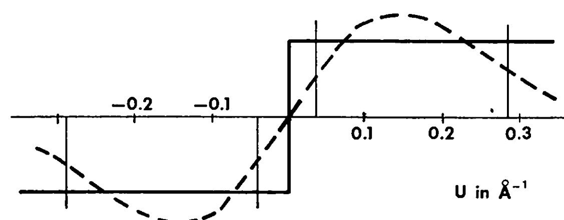

Fig. 3. The approximation to a step function by means of the differential of a Gaussian.

As a critical test of the expressions (17) and (18) we consider again the simple test object having

$$\varphi(xy)=A+B\cos(2\pi x/a)\,.$$

Use of a displaced aperture will remove two of the three δ-function peaks in the back focal plane. Then in the image plane we should have

$$\psi(xy)=\tfrac{1}{2}B[\cos(2\pi x/a)-i\sin(2\pi x/a)] \tag{19}$$

and $I(xy)=B^2/4$.

The use of equation (17) gives a different form for the amplitude for each periodicity but this can be made close to (19) in the range of interest. For example, for

$$a=15\ \text{Å},\ \psi(xy)=\tfrac{1}{2}B[\cos(2\pi x/a)-i\ 0{\cdot}96\sin(2\pi x/a)]\,,$$
$$a=10\ \text{Å},\ \psi(xy)=\tfrac{1}{2}B[\cos(2\pi x/a)-i\ 1{\cdot}28\sin(2\pi x/a)]\,,$$
$$a=5\ \text{Å},\ \psi(xy)=\tfrac{1}{2}B[\cos(2\pi x/a)-i\ 1{\cdot}20\sin(2\pi x/a)]\,,$$
$$a=4\ \text{Å},\ \psi(xy)=\tfrac{1}{2}B[\cos(2\pi x/a)-i\ 0{\cdot}84\sin(2\pi x/a)]\,.$$

For more general types of object it might be expected that the defects of this simple model might be less obvious.

5. Dark field with small apertures

For a great deal of work on crystals, including the study of crystal defects, dark-field images are frequently obtained using a relatively small aperture centered at a distance from the central beam which is large compared with its diameter, as suggested in Fig. 2(*c*). The purpose is usually to find the distribution or form of the part of the specimen giving rise to a particular feature of the diffraction pattern and the method has most frequently been applied to the study of crystals which are too thick to be considered within the framework of the phase-object approximation and where considerations of high resolution are not involved. However there are some cases of this sort where our treatment is relevant and these will be considered briefly below.

For these cases there seems to be little point in attempting extensions of the previous sections and each case must be treated individually.

(*a*) *A diffracted beam and surrounding scattering*

To a reasonable approximation a strong diffracted beam from a thin crystal can be considered as a re-

directed plane incident wave. The diffraction spot is surrounded by scattering corresponding to the shape transform of the regions giving the diffracted beam. Hence under the 'high-resolution dark-field' conditions with the incident beam tilted so that the diffracted beam is axial, the imaging resembles bright-field imaging with the important difference that the incident beam δ function, $\pi/2$ out of phase with the first-order scattered radiation, is missing. Hence the optimum defocus position is such that $\chi \simeq 0$ for the largest possible area of the back focal plane. For the conditions of Fig. 1 this implies optimum imaging for 300-400 Å underfocus.

(b) Several diffracted beams from one crystal

Images of crystal lattices showing the periodicity of the unit cell may be obtained when the objective aperture transmits more than one diffraction spot from the crystal. It is readily shown that the intensity distribution within the unit-cell periodicity will in general bear no simple relationship to the crystal structure. In the limiting case of very thin crystals and first-order scattering only, the intensity distribution in the image will be, from (9),

$$I(xy) = \psi\psi^*(xy) = \left| \sum_h' \sum_k' \Phi_{hk} \exp\{i\chi_{hk}\} \times \exp\left\{2\pi i \left(\frac{hx}{a} + \frac{ky}{b}\right)\right\}\right|^2 \quad (21)$$

where the primes on the summations indicate that only spots transmitted by the aperture are included and χ_{hk} is the value for the hk reflection. With increasing crystal thickness the first-order scattering theory fails (for 10–50 Å thickness for medium-weight atoms) and the relation of image to crystal structure rapidly becomes more complicated.

(c) Diffuse scattering from disorder or defects in crystals

If the objective aperture excludes all diffraction spots given by a crystal and transmits only the diffuse scattering due to defects or disorder, involving displacement or replacement of atoms, the image may provide information regarding the nature and form of the deviations from the periodicity of the crystal. This dark-field method is becoming of increasing importance for defect and disorder studies and will be treated in detail in a further paper of this series. We limit ourselves here to a brief summary.

The diffuse scattering is given, kinematically, by the deviations from the average periodic structure. Hence we write

$$\varphi(xy) = \bar{\varphi}(xy) + \Delta\varphi(xy) , \quad (22)$$

where $\bar{\varphi}$ is the average, periodic structure and the non-periodic deviation $\Delta\varphi$ is defined so that $\langle\Delta\varphi\rangle = 0$. Then the image intensity in the ideal-case dark-field situation will be given by

$$I(xy) = |\Delta\varphi(xy)|^2 . \quad (23)$$

Hence both positive and negative deviations from the average structure will give intensity maxima.

The same considerations apply to the images obtained from diffuse scattering from amorphous or semicrystalline materials where the deviation from the average potential, $\Delta\varphi$, may be identified with $\varphi(xy) - \bar{\varphi}$, considered in §§ 3 and 4 above. The small size of the aperture assumed in the present case generally precludes the resolution of unit cell periodicities.

Further complication arise when the magnitude of the deviations $\Delta\varphi(xy)$ is such that it cannot be assumed that $\sigma\Delta\varphi(xy) < 1$, or when strong dynamical scattering of reflections from an average periodic lattice modifies the diffuse scattering.

6. Phase objects with large phase changes

Particularly in the presence of atoms of medium or high atomic number and for crystalline specimens, the values of $\sigma\varphi(xy)$ may greatly exceed unity within the thickness range for which the phase object approximation (1) is valid. Then the approximation leading to (5) cannot be used and we must write instead,

$$q(xy) = \cos \sigma\varphi(xy) - i \sin \sigma\varphi(xy) ,$$
$$\psi(uv) = C(uv) \cos \chi - S(uv) \sin \chi - i[C(uv) \sin \chi + S(uv) \cos \chi] , \quad (24)$$

where $C(u)$ and $S(u)$ are the Fourier transforms of $\cos \sigma\varphi(xy)$ and $\sin \sigma\varphi(xy)$ and are real functions only if $\sigma\varphi(xy)$ has a center of symmetry, which we may assume for convenience. It is then difficult to comprehend the form of the resulting bright-field or dark-field images without extensive computing for each particular object. For imaging with limited resolution (spherical aberration not important) one may use the approximation of Cowley & Moodie (1960) that the contrast for small defocus is proportional to the projected charge density (see Anstis, Lynch, Moodie & O'Keefe, 1973). The very approximate treatment of bright-field imaging of thin crystals given by Cowley & Iijima (1972) suggests that, under the optimum defocus conditions, the image will give much the same representation of the projected structure as for small phase changes with the important difference that with increasing phase change (or for increasing thickness of crystals seen in principal orientations) the maxima of image contrast cease to increase proportionately. This behavior has been confirmed for particular crystals by computations of image intensities using complete n-beam dynamical diffraction theory (Fejes, 1972; O'Keefe, 1972), which showed excellent agreement with the experimental observations of Iijima (1971).

For dark-field imaging we may obtain relatively simple expressions for the intensity if we make the approximation used above that, for the optimum de-

focus, $\chi \simeq 0$ so that

$$\psi(uv) = C(uv) - iS(uv)\,. \qquad (25)$$

For the ideal dark-field conditions with a small central stop we assume that only the zero beam is excluded. This has amplitude $C_0 - iS_0$, where

$$C_0 = \frac{1}{A}\int \cos \sigma\varphi(xy)\mathrm{d}x\mathrm{d}y$$

$$S_0 = \frac{1}{A}\int \sin \sigma\varphi(xy)\mathrm{d}x\mathrm{d}y \qquad (26)$$

where A is the area of integration.

The image amplitude and intensity are then

$$\psi(xy) = [\cos \sigma\varphi(xy) - C_0] - i[\sin \sigma\varphi(xy) - S_0]\,, \qquad (27)$$

$$I(xy) = (1 + C_0^2 + S_0^2) - 2[C_0 \cos \sigma\varphi(xy) + S_0 \sin \sigma\varphi(xy)]\,. \qquad (28)$$

It can be seen that for small $\sigma\varphi$ values (27) and (28) reduce to (11) and (12) respectively.

For an intermediate stage of approximation we may write that, for the ideal dark-field image

$$\begin{aligned}\psi(xy) &= \exp\{-i\sigma\varphi(xy)\} - \overline{\exp\{-i\sigma(xy)\}} \\ &= \exp\{-i\sigma\bar{\varphi}\}[\exp\{-i\sigma\{\varphi-\bar{\varphi}\}\} \\ &\quad - \overline{\exp\{-i\sigma(\varphi-\bar{\varphi})\}}]\,. \end{aligned} \qquad (29)$$

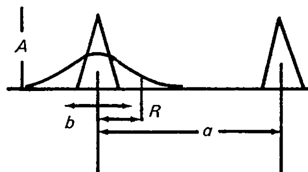

$\frac{b}{a} = \frac{1}{10}$ $\qquad \frac{a}{\sqrt{\pi}R} = 3$

Fig. 4. Model object with projected potential in the form of triangular peaks. The coherent loss of resolution is given by convolution with a Gaussian of half-width R.

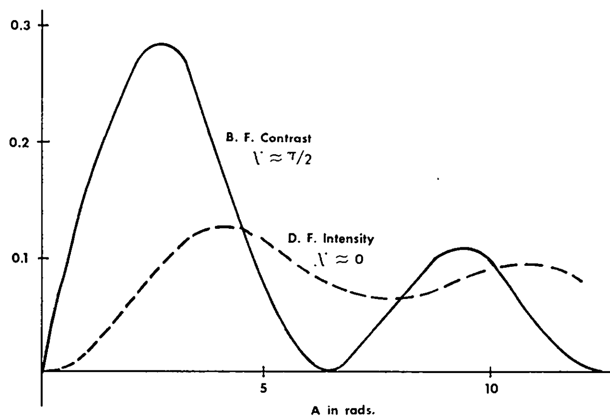

Fig. 5. Bright-field contrast and dark-field intensity (arbitrary scale) calculated for the model object of Fig. 4 as a function of the peak phase change in radians.

But

$$\overline{\exp\{-i\sigma(\varphi-\bar{\varphi})\}} = 1 - i\sigma\overline{(\varphi-\bar{\varphi})} - \frac{\sigma^2}{2!}\overline{(\varphi-\bar{\varphi})^2}$$

$$\simeq \exp(-M) \text{ where } M = \tfrac{1}{2}\sigma^2\overline{(\varphi-\bar{\varphi})^2},$$

so that

$$I(xy) \simeq 1 + \exp\{-2M\} - 2\exp\{-M\}\cos \sigma(\varphi - \bar{\varphi})\,. \qquad (30)$$

This suggests that the intensity is given by (12) if $\sigma(\varphi - \bar{\varphi})$ is small but as this quantity increase the intensity oscillates about a limiting value. In order to deal with the cases of translated-aperture or 'high-resolution' dark field, we may apply the approximations used in § 4 above. As before, we have the relationship that, if the 'ideal' dark-field amplitude is ψ_0, then

$$\psi(xy) = \tfrac{1}{2}\psi_0(xy) + \frac{i}{\pi}\,C_1 \frac{\partial}{\partial x}\,\psi_0(xy) \qquad (31)$$

where C_1 is the constant of (17) and we have omitted the convolution with the Gaussian.

Applying this to ψ_0 from (27) we obtain

$$\psi(xy) = \left[\left(1 - \frac{C_1}{\pi}\sigma\varphi'\right)\cos \sigma\varphi - C_0\right] + i\left[\left(1 - \frac{C_1}{\pi}\sigma\varphi'\right)\sin \sigma\varphi - S_0\right], \qquad (32)$$

and

$$\psi\psi^*(xy) = \left[1 - \frac{C_1}{\pi}\sigma\varphi'\right]^2 + C_0^2 + S_0^2 - 2\left(1 - \frac{C_1}{\pi}\sigma\varphi'\right)[C_0 \cos \sigma\varphi + S_0 \sin \sigma\varphi]\,, \qquad (33)$$

where the prime on φ' indicates the differential.

7. An example

Although it is not possible to find simple analytical forms for expressions such as (28) and (33) in general, this can be done for a few model objects. For example we consider the periodic object with triangular peaks of potential represented in Fig. 4. Peaks of total width b and height A are repeated at distances a. There is a coherent loss of resolution due to aperture limitation represented by convolution of the image amplitude by a Gaussian of half-width R. We assume $a > R \gg b$.

To calculate dark-field intensity for the central-stop case we assume $\chi \simeq 0$ and obtain, in reasonable approximation,

$$I_{\mathrm{DF}}(xy) = \frac{b^2}{a^2}\left[1 - \frac{a}{\sqrt{\pi R}}\exp\{-x^2/R^2\}\right]^2 \times \left[\left(1 - \frac{\sin A}{A}\right)^2 + \left(1 - \frac{\cos A}{A}\right)^2\right]. \qquad (34)$$

In Fig. 5 the values of peak dark-field intensity are plotted as a function of A, the maximum phase change measured in radians, for $b/a = 0{\cdot}1, a/\pi R = 3$. It is seen

that the inital parabolic shape of the curve is soon lost and the peak intensity appears to oscillate about a constant value for large A. In this respect the behavior is similar to that previously found for bright-field contrast (Cowley & Iijima, 1972) and will lead to the same sort of considerations for the interpretation of crystal lattice images. The approximation of equation (30) is seen to be an improvement on that of equation (12).

8. Conclusions

It is evident that the assumption that dark-field images may be simply interpreted in terms of a density of scattering matter is usually far from being correct for high-resolution imaging of thin objects. We have shown that under the optimum defocus conditions it is possible to obtain a relatively simple expression for the image intensity for the case of very small phase change and an indication of the behavior with increasing phase change. However the intensity does not depend directly on the density of scattering matter, but rather depends on the square of the deviation from an average value of the projected potential. Positive and negative deviations will give the same intensities so that, for example, a hole and a heavy-atom inclusion in a light-atom matrix could give the same contrast.

As in bright-field imaging, the possibility of interpreting the image intensity in a reasonably straightforward way depends on obtaining the correct amount of defocus. As can be deduced readily from the curves of Fig. 1 taken in conjunction with equation (5), the relative phase of the different parts of the diffraction pattern may be varied through large angles by change of R. However, this dependence is less severe than for a bright-field image because for small defocus the main weighting factor for the amplitudes is the $\cos\chi$ function which varies less rapidly than $\sin\chi$. For example for $u \le 0{\cdot}13$ (*i.e.* for a resolution of 7 Å) the change of R from 0 to 400 Å will not make much difference to the dark-field image under the conditions for which Fig. 1 applies.

For dark-field images which can be easily interpreted the maximum aperture size which can be used is less than for bright field. From Fig. 1(a), the optimum defocus dark-field condition applies for $|U| \le 0{\cdot}20$ whereas for bright field it is possible to use $|U| \le 0{\cdot}28$. However, in bright-field imaging the most important interference process is between the diffracted beam and the incident beam, with a maximum difference in U of $U_{\max}(=0{\cdot}28\ \text{Å}^{-1})$; in dark field the primary interference is between diffracted beams which may be separated by $2U_{\max}(=0{\cdot}40\ \text{Å}^{-1})$. Hence the dark-field image may show detail on a finer scale and so have a better 'resolution' in some cases.

For the practical application of dark-field images there is the important experimental problem of determining the defocus distance, since the minimum contrast criterion for determining exact focus for bright field does not apply, and Fresnel fringes are not usually visible. Some criteria for obtaining optimum focus will be discussed in a future publication.

All the above considerations of image contrast may be seen to apply equally to the appropriate configurations for scanning transmission electron microscopy by application of the reciprocity relationship (Cowley, 1969) and, by extension, the necessary modifications of the simple theory which has been applied to the ratio-signal imaging scheme of Crewe *et al.* (1970) may be inferred.

This work was supported by a grant from the National Institute for General Medical Sciences, GM 18204. The author is grateful to Dr Robert Glaeser for some critical comments on the manuscript.

References

Anstis, G. R., Lynch, D. F., Moodie, A. F., & O'Keefe, M. A. (1973). *Acta Cryst.* A**29**, 138–147.

Cowley, J. M. (1969). *Appl. Phys. Lett.* **15**, 58–59.

Cowley, J. M. & Iijima, S. (1972). Z. *Naturforsch.* **27*a***, 445–451.

Cowley, J. M. & Moodie, A. F. (1960). *Proc. Phys. Soc.* **76**, 378–384.

Crewe, A. V. & Wall, J. (1970). *Optik*, **30**, 461–74.

Dupuoy, G., Perrier, F. & Durrieu, L. (1970). *J. Microsc.* **9**, 575–592.

Eisenhandler, C. B. & Siegel, B. M. (1965). *J. Appl. Phys.* **37**, 1613–1620.

Erickson, H. P. & Klug, A. (1970). *Phil. Trans.* B**261**, 105–118.

Fejes, P. L. (1972). *Proceedings*, 30*th Annual Meeting, EMSA*, pp. 558–559. Edited by C. J. Arcenaux. Claitors Publ. Div.

Formanek, H., Muller, M., Hahn, M. H. & Koller, T. (1971). *Naturwissenschaften*, **58**, 339–344.

Grinton, G. R. & Cowley, J. M. (1971). *Optik*, **34**, 221–233.

Hashimoto, H., Kumao, H., Hino, K., Yotsumoto, H. & Ono, A. (1971). *Jap. J. Appl. Phys.* **10**, 1115–1116.

Heidenreich, R. D. & Hamming, R. W. (1965). *Bell Syst. Tech. J.* **44**, 207–233.

Heinemann, K. & Poppa, H. (1970). *Appl. Phys. Lett.* **16**, 515–516.

Iijima, S. (1971). *J. Appl. Phys.* **42**, 5891–5893.

Massover, W. H. (1972). *Proceedings*, 30*th Annual Meeting EMSA*, pp. 182–183. Edited by C. J. Arcenaux. Claitors Publ. Div.

O'Keefe, M. (1972). M. Sc. Thesis, University of Melbourne

Scherzer, O. (1949). *J. Appl. Phys.* **20**, 20–29.